

# Effects of farnesol on the physical properties of DMPC membranes

Amy C. Rowat, Danielle Keller, John H. Ipsen\*

Department of Physics, University of Southern Denmark, MEMPHYS-Center for Biomembrane Physics, Campusvej 55, DK-5230 Odense M, Denmark

Received 28 February 2005; received in revised form 12 April 2005; accepted 29 April 2005

Available online 31 May 2005

## Abstract

Farnesol interacts with membranes in a wide variety of biological contexts, yet our understanding of how it affects lipid bilayers is not yet complete. This study investigates how the 15-carbon isoprenoid, farnesol, influences the phase behaviour, lateral organization, and mechanical stability of dimyristol phosphatidylcholine (DMPC) model membranes. Differential scanning calorimetry (DSC) of multilamellar DMPC–farnesol mixtures (up to 26 mol% farnesol) demonstrates how this isoprenoid lowers and broadens the gel–fluid phase transition. A gel–fluid coexistence region becomes progressively more dominant with increasing farnesol concentration and at concentrations of and greater than 10.8 mol%, an upper transition emerges at about 35 °C. Atomic force microscopy images of supported farnesol–DMPC bilayers containing 10 and 20 mol% farnesol provide structural evidence of gel–fluid coexistence around the main transition. Above this coexistence region, membranes exhibit homogeneous lateral organization but at temperatures below the main gel–fluid coexistence region, another form of phase coexistence is observed. The solid nature of the gel phase is confirmed using micropipette aspiration. The combined thermodynamic, structural, and mechanical data allow us to construct a phase diagram. Our results show that farnesol preferentially partitions into the fluid phase and induces phase coexistence in membranes below the main transition of the pure lipid.

© 2005 Elsevier B.V. All rights reserved.

**Keywords:** DSC; AFM; Phase behaviour; Mechanics; Lateral organization; Lipid bilayer; Isoprenoid

## 1. Introduction

Farnesol is a 15-carbon (C<sub>15</sub>) isoprenoid (Fig. 1) and a natural component of many plant oils that is active in a large number of biological contexts: it mimics the female bee's sex pheromone in the early spider orchid [1], is a regulator of apoptosis [2,3], has a pronounced ability to dietarily combat pancreatic cancer growth [4], and has also been demonstrated to have antibacterial activity and reduce biofilm viability [5,6]. Farnesol is the dephosphorylated form of farnesyl pyrophosphate, a compound that is common to all branches of the mevalonate pathway and thus precursor of sterols, dolichol, vitamins E and K1, and prenylated proteins. Besides being an important biosynthetic intermediate, increasing evidence suggests that farnesol itself plays a direct role in membrane-associated biological function.

Various lines of evidence indicate the membrane-related activity of farnesol. Farnesol has nonspecific effects on a variety of ion channels [7,8]. Also, the posttranslational attachment of the farnesyl chain to proteins that are important in cell signalling and function such as p21ras, nuclear lamins, and fungal mating factors, is crucial for their membrane association and biological function [9]. Not only does farnesol mediate the association of proteins with membranes, it also acts to regulate the lateral organization of proteins in the plane of the membrane. Prenylated proteins and peptides have been observed to be excluded from more ordered domains enriched in cholesterol and sphingolipids in both model and biological systems [10–13]. Proteins modified by saturated acyl chains, on the other hand, are targeted to these more ordered domains. Much research activity has been devoted to understanding how cholesterol, sphingolipids, and saturated acyl chains affect membrane properties and lateral organization, but relatively little is known of the effects of members of the prenyl family, including farnesol. A better understanding of the mecha-

\* Corresponding author. Tel.: +45 6550 2560; fax: +45 6615 8760.

E-mail address: [ipsen@memphys.sdu.dk](mailto:ipsen@memphys.sdu.dk) (J.H. Ipsen).

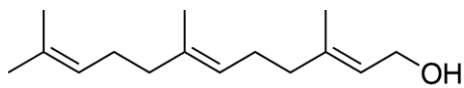


Fig. 1. Structure of *trans-trans* farnesol (3,7,11-trimethyl-2,6,10-dodecatriene-1-ol).

nisms involved in lateral phase segregation and domain formation requires more detailed knowledge of farnesol–membrane behaviour and organization.

Farnesol's amphiphilic nature suggests that it naturally solubilizes into membranes. Various studies attest to the integration of isoprenoid probes including farnesol into model membranes [14–17]. Calorimetry and 1,6-diphenyl-1,3,5 hexatriene (DPH) fluorescence [18] show that farnesol stabilizes the fluid phase. A study of farnesol–DMPC phase behaviour using deuterium nuclear magnetic resonance ( $^2\text{H}$  NMR) also revealed that farnesol stabilizes the fluid phase and thereby decreases and broadens the main gel–fluid phase transition [19]. Farnesol has been observed to have only negligible effects on membrane mechanical stability in the fluid phase as values of the membrane bending rigidity modulus in the fluid phase remain largely unaffected by the presence of up to 25 mol% farnesol [20]. These studies raise questions of exactly how farnesol interacts with lipid membranes. Specifically, spectroscopy measurements reveal that order parameters remain unaffected by the presence of farnesol above the coexistence region and suggest that the phase below the coexistence region is more fluid in character. Based on  $^2\text{H}$  NMR data, a partial phase diagram for DMPC-farnesol has been proposed [19] but complementary structural data is lacking. Both the nature of farnesol–lipid phases and phase diagram topology has thus remained unresolved.

In this study, we seek to answer these questions and attain a more complete knowledge of farnesol–membrane behaviour. To achieve this, we investigate the thermodynamics, lateral organization, as well as membrane mechanics of farnesol–DMPC mixtures. Differential scanning calorimetry (DSC) has facilitated an extended analysis of DMPC–farnesol phase behaviour at concentrations up to 26 mol%. Complementary atomic force microscopy (AFM) images provide visual evidence of membrane lateral organization. These studies show that farnesol lowers DMPC's main gel–fluid transition temperature,  $T_m$ , and induces gel–fluid phase coexistence around the main transition. At concentrations at and above 10.8 mol%, an upper transition emerges at about 35 °C. With the inclusion of more than 19 mol% farnesol in membranes, the transition appears as a very broad endotherm and the transition temperature remains independent of farnesol concentration. To test membrane mechanical properties in the gel phase region, micropipette aspiration was used to deform vesicles. This demonstrates that below and near the solidus boundary of the main coexistence region, membranes exhibit shear rigidity characteristic of the gel phase. Compiling thermodynamic,

structural, and mechanical data, we construct a farnesol–DMPC phase diagram. The main gel–fluid coexistence region predominates the phase diagram. Above this phase region, homogeneous membrane organization is observed while below this region, we see evidence of a different form of phase separation that further supports farnesol's preferential partitioning into the fluid phase. Our observations that membrane stability remains largely unperturbed by the presence of farnesol and that farnesol demonstrates affinity for the fluid phase may be significant for the membrane association, lateral organization, and function of prenylated proteins.

## 2. Methods

### 2.1. Materials

DMPC (dimyristoylphosphocholine) was obtained from Avanti Polar Lipids Inc. (Alabaster, Alabama) and *trans-trans* farnesol (96% pure) and solvents from Sigma-Aldrich (Copenhagen, Denmark). Di-I-C18 (1,1'-dioctadecyl-3,3,3',3'-tetramethylindocarbocyanine perchlorate) was a product of Molecular Probes (Eugene, Oregon).

### 2.2. Bounds of the partition coefficient

Farnesol was observed to have an extremely low solubility in water. A small drop of farnesol (7.9 mg) was diluted and vigorously shaken in progressively larger volumes of water. Even in 5.0 l of water (a concentration of  $3.5 \times 10^{-5}$  M), an insoluble drop of farnesol visibly remained on the surface. The fraction of farnesol in the water phase is thus expressed as follows:  $X_{\text{H}_2\text{O}}^{\text{fsl}} = n_{\text{fsl}} / (n_{\text{fsl}} + n_{\text{H}_2\text{O}}) \ll 1 \times 10^{-7}$ . Upon the addition of 5.7 mg farnesol to 196.3 mg of a 25-mM DMPC dispersion (100 nm unilamellar liposomes in water) and repeated shaking, no surface droplets were observed. This suggests that farnesol preferentially partitions into the lipid phase. The limiting molar fraction of farnesol in the lipid phase is written as:  $X_{\text{lipid}}^{\text{fsl}} = n_{\text{fsl}} / (n_{\text{fsl}} + n_{\text{lipid}}) < 5 \times 10^{-3}$ . A lower bound on the partition coefficient,  $K_p$ , is estimated as:  $K_p = X_{\text{lipid}}^{\text{fsl}} / X_{\text{H}_2\text{O}}^{\text{fsl}} \gg 4 \times 10^4$ .

Our estimates of farnesol's large partition coefficient were confirmed via a membrane partitioning assay as previously described [21]. This affirms that farnesol has an extremely high affinity for the lipid membrane. The concentration of farnesol in solution is thus an accurate representation of the amount of farnesol contained within the membrane.

### 2.3. DSC

Varying concentrations of farnesol were dissolved with DMPC in ethanol ( $X_{\text{fsl}}$  from 2.9–26.4 mol%, where  $X_{\text{fsl}} = n_{\text{fsl}} / (n_{\text{fsl}} + n_{\text{DMPC}})$ ). The organic solvent was

evaporated for at least 12 h under vacuum. MilliQ water (Millipore, Bedford, Massachusetts) was added to yield a multilamellar dispersion with a total lipid concentration of 1.5 mM. Six DSC scans (heating and cooling) were run from 5 to 40 °C at a scanning rate of 10 °C/h (Nano-DSC II, Calorimetry Sciences Corp, Provo, Utah). At least two independent measurements were obtained for each farnesol concentration.

A consistent choice of baseline is necessary for determining both phase boundaries at differing compositions and for a consistent comparison of transition enthalpies. Our strategy for making baselines is as follows: as the transition region is approached from below or above, the baseline is chosen to end at the temperature where  $|\frac{dC_p}{dT}|$  is doubled over the temperature range  $\Delta t_s = 0.05$  °C; i.e.,  $|\frac{dC_p}{dT}|_{t+\Delta t_s} = 2 |\frac{dC_p}{dT}|_t$ . The analysis of  $\Delta H$  is based on this procedure of baseline determination.

In constructing a phase diagram, the solidus and liquidus phase boundaries can be determined by discerning the temperature of the onset and completion of the transition ( $\tau_1$  and  $\tau_2$ ) from the experimental  $C_p$  curves. Traditionally these temperatures are determined to be where the experimental curve deviates from the thermogram baseline [22]. We have chosen the temperature of the onset of the transition to be where the lower baseline ends and the peak of the main transition to be a good approximation of where the  $C_p$  peak ends. In cases where a defined shoulder grows on the upper side of the  $C_p$  peak (at 10.8 mol% and above), the point where the shoulder meets the baseline is chosen to be the upper boundary of what we denote as the  $\gamma$ -region.

#### 2.4. AFM

Lipid–farnesol dispersions were prepared as described above to a final lipid concentration of 1.5 mM. The sample was vigorously shaken and then incubated in a water bath for 45 min at 37 °C before extrusion ten times through two stacked polycarbonate filters (100 nm pore size, Whatman, Middlesex, UK). The solution was deposited onto a piece of freshly cleaved mica (ruby muscovite mica, Plano GmbH, Wetzlar, Germany) and incubated overnight at 4 °C. The following day, the sample was washed seven times with milli-Q water and incubated at 40 °C for 30 min. After incubation, the sample was immediately cooled down to 6 °C and mounted in a homemade fluid cell equipped with a thermocouple to measure the temperature inside the cell. Images were acquired in magnetic AC (MAC) mode in a picoSPM atomic force microscope (Molecular Imaging, Tempe, Arizona). The AFM tips were MAClevers type II with a resonance frequency of  $\sim 25$  kHz in water and a nominal spring constant of 2.8 N/m. During the experiments, the temperature was adjusted with a Lakeshore model 330 temperature controller (Lake Shore Cryotronics Inc, Westerville, Ohio). In a heating experiment, the temperature was changed in steps of one to

three °C. After changing the temperature, the sample was scanned until the temperature was stable and the sample had equilibrated (image appearance no longer changed). The samples were scanned continuously for approximately 6 h and care was taken that they remained hydrated throughout an experiment. At least three different samples for each membrane composition were observed in independent experiments.

Phase boundaries for the supported DMPC–farnesol membranes were determined by visual inspection of the AFM images. The lower phase boundary was defined as the temperature where the membrane begins to melt and broadening of the grain boundaries is observed. The fluidus boundary was determined to be at the temperature where signs of the elevated gel phase disappear.

#### 2.5. Micropipette aspiration

Solutions of 0.30 mM DMPC containing 10 and 20 mol% farnesol and 0.5 mol% Di-I-C18 in chloroform were prepared and 8  $\mu$ l of the lipid mixture was deposited on platinum wire electrodes using a Hamilton syringe. The solvent was subsequently evaporated overnight in a vacuum chamber. Giant unilamellar vesicles (GUVs) were formed by electroformation [23,24] in a  $\approx 200$  mOsm sucrose solution at 40 °C, well above  $T_m = 23.9$  °C of pure DMPC. The vesicles were then resuspended in a  $\approx 200$  mOsm glucose solution contained in the thermostated observation chamber. Solution osmolarities were regulated using a freezing-point osmometer (Model 3D3, Advanced Instruments Inc, Norwood, Massachusetts) and MilliQ water was used throughout (Millipore, Bedford, Massachusetts). Vesicles from at least three independently prepared batches were tested.

### 3. Results and discussion

#### 3.1. Effects upon phase transitions: thermodynamics

Fig. 2 illustrates a series of heating scans for DMPC–farnesol mixtures up to 26 mol% obtained using DSC. The most striking feature of the series of thermograms is that the main phase transition for DMPC—represented by the peak in  $C_p$ —is progressively lowered and broadened with increasing concentrations of farnesol. The position of the main peak is reduced from  $T_m = 23.9$  °C for DMPC down to about 19.7 °C with 19 mol% farnesol. At farnesol concentrations above 19 mol%, the position and shape of the thermogram peak is nearly invariant.

Immediately above the position of the main peak, a small “shoulder” begins to emerge at concentrations of 2.9 mol% farnesol. This shoulder expands with increasing farnesol content and becomes more defined in shape at and above 10.8 mol%. At similar concentrations in the temperature range of 35–37 °C, a small endothermic peak

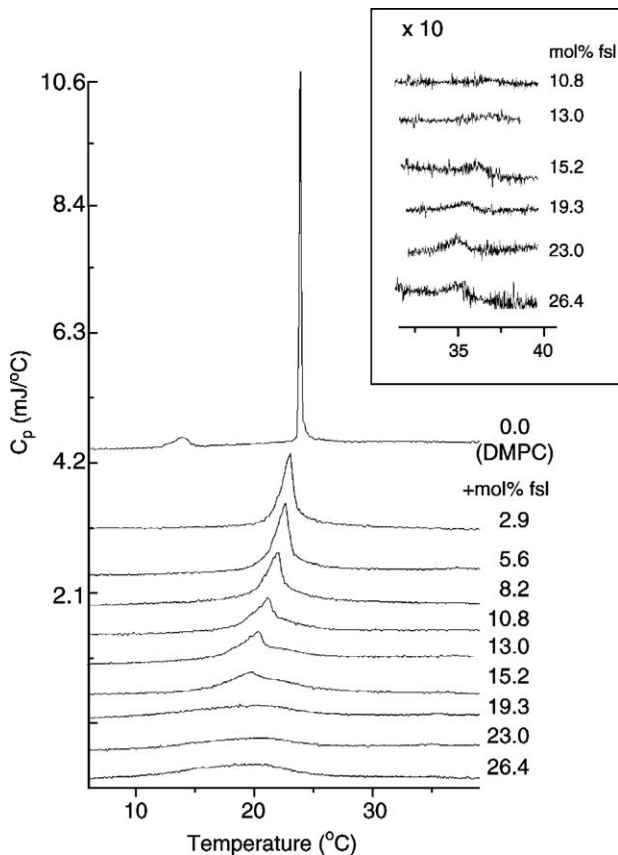


Fig. 2. DSC heating scans of DMPC multilamellar vesicles containing increasing concentrations of farnesol. Displayed in the inset is a magnification of the upper transition.

appears in the  $C_p$  scans, the origin of which is uncertain. No significant broadening of this peak is observed with increasing farnesol content, but a modest decrease of this transition temperature is observed (Fig. 2, inset). DSC scans of the samples in the absence of lipids reveal that farnesol alone exhibits no transitions in the same temperature range (not shown).

Well below the main phase transition temperature, signs of the pretransition are quickly abolished by the presence of farnesol. At 2.9 mol%, farnesol lowers the pretransition from 14 to 7 °C (not visible in Fig. 2) and with a concentration of 5.6 mol%, there is no longer any sign of the pretransition in the temperature range investigated. The vanishing cooperativity of the pretransition is common upon the addition of membrane solutes [25,26].

### 3.2. Visualizing farnesol–DMPC membranes

Visual evidence of farnesol–DMPC lateral organization is provided by AFM images of DMPC bilayers on mica substrates containing 10 and 20 mol% farnesol. Image acquisition was begun at low temperatures and the temperature was gradually increased in increments.

In the initial state at lower temperatures, the bilayers typically have holes (Figs. 3A and 4A). Holes are

commonly observed in supported lipid bilayers [27]. The depth of the holes is  $43 \pm 1$  Å corresponding to the thickness of the bilayer in the solid phase and a very thin water film between the bilayer and the mica support. Phase imaging shows a large phase difference between the top of the bilayer and the bottom of the holes (not shown) which indicates that there is only one bilayer supported directly on the mica surface.

The two lipid–farnesol compositions investigated by AFM in this study both exhibit phase transitions that occur at different temperatures in the two monolayers and at elevated temperatures relative to the DMPC–farnesol suspensions investigated by DSC. This is a phenomenon previously observed in mica-supported bilayers [27,28].

#### 3.2.1. 10 mol% farnesol

At temperatures below  $T_m$ , DMPC+10 mol% farnesol bilayers exhibit a lateral structure of lines (grain boundaries) connecting the holes (Fig. 3A). When the temperature is increased, the holes shrink in size due to lateral bilayer expansion. Furthermore, the lines become wider indicating that the bilayers start to melt at these boundaries (Fig. 3B). Gel–fluid phase coexistence is clearly observed in Fig. 3C where the height difference between the two phases is 7–8 Å. Upon increasing the temperature, the fluid phase expands at the expense of the gel phase until the entire upper leaflet is fluid (Fig. 3D). At higher temperatures, both leaflets of the membrane become fluid. This is reminiscent of a gel-connected to fluid-disconnected transition which has previously been described in the literature [29] and observed by AFM [30]. The shape of these domains is similar to that observed in previous studies of coexisting gel and fluid phases [27,31].

#### 3.2.2. 20 mol% farnesol

In contrast to the DMPC+10 mol% farnesol bilayers, DMPC bilayers containing 20% farnesol exhibit phase coexistence at temperatures well below  $T_m$  of the pure lipid (Fig. 4A) where the bilayer is expected to be completely in a gel phase ( $T=8.8$  °C). Distinct from typical gel–fluid coexistence, the height difference between these two phases is 13–14 Å and the domain shape is relatively more round (Fig. 4B). When the temperature is increased, the holes begin to expand. At the same time, the fluid areas gradually disappear (Fig. 4C) until a gel phase bilayer with a network of lines, similar to the one observed in DMPC+10 mol% farnesol membranes, has formed (Fig. 4D). Further increasing the temperature leads to a phase transition like that observed in DMPC+10 mol% farnesol bilayers where the transition is initiated at the lines (Fig. 4D) and two coexisting phases emerge with a height difference of 7–8 Å. The domain shape is also similar to that seen in DMPC+10 mol% farnesol (Fig. 4F) and is characteristic of gel–fluid coexistence. This coexistence persists until the top monolayer (Fig. 4G) and then the entire bilayer becomes fluid (Fig. 4H).

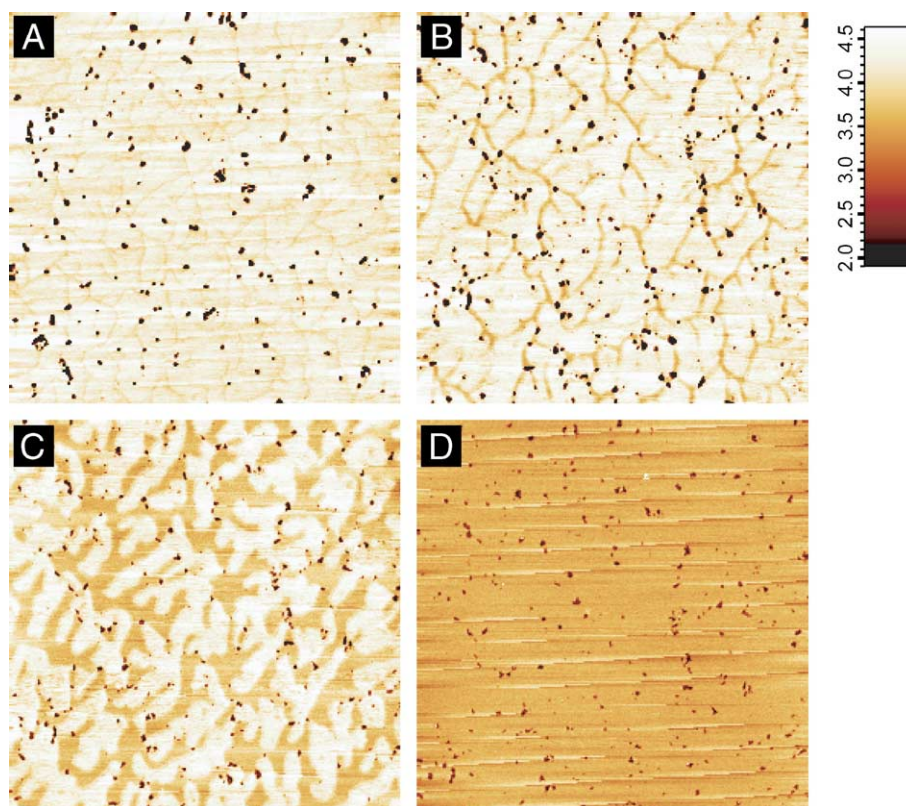


Fig. 3. AFM images of mica-supported DMPC+10 mol% farnesol bilayers. The organization changes with temperature: A: 12 °C (gel phase); B: 20 °C (close to the solidus line); C: 23 °C (gel–fluid phase coexistence); and D: 28 °C (top monolayer in the fluid phase). All images are  $5 \times 5 \mu\text{m}^2$ .

### 3.3. Transition enthalpies

The transition enthalpy,  $\Delta H$ , of the main phase transition can be determined from the DSC data. The obtained transition enthalpies are shown in Table 1 where  $\Delta H$  per mole of both DMPC and total membrane molecules is shown as a function of the membrane composition. Only the contributions to the enthalpy around the main transition are shown. After an initial increase,  $\Delta H$  stabilizes at a value slightly larger than  $\Delta H$  for the main phase transition of pure lipid and modestly decreases with  $X_{\text{fsl}} \geq 19$  mol%. In the temperature range of 35–37 °C, an endothermic peak appears in the  $C_p$  scans at farnesol concentrations greater than 15.2 mol%. In comparison to the enthalpy of the main transition, the heat content of this transition is very small ( $\Delta H \leq 418$  kJ/mol).

### 3.4. Signs of shear rigidity below the main coexistence region

Various lines of evidence motivated us to question the nature of the phase below  $T_m$  of the pure lipid where the bilayer is expected to be in a gel phase with properties of a solid. In this phase region, lateral phase separation is observed by AFM and spectroscopy reveals that fluid phase characteristics (reduced order and/or different types and rates of motion) persist [18,19]. To further investigate the

nature of this phase, we performed a simple test of deforming GUVs using micropipette aspiration.

Upon aspiration of a pure DMPC GUV at temperatures above  $T_m$ , the vesicle readily extends into the pipette at relatively low pressures (0.5–3 kPa). Upon expiration of deformed fluid phase vesicles, they are observed to return to their original quasi-spherical shape on short timescales (on the order of seconds). Well below the phase transition of the pure lipid (15 °C), however, aspirated DMPC GUVs are observed to retain deformations upon expiration. Such vesicles also withstand much larger pressures under which fluid vesicles typically lyse (5–7 kPa). The mechanism of failure of gel-state membranes also reveals characteristics of a solid: buckling folds form and the vesicle collapses. These folds persist upon expiration signalling the solid-like nature of the membrane.

Similar to pure DMPC vesicles, GUVs containing 10 and 20 mol% farnesol were observed to exhibit fluid-like behaviour above the main transition temperature. In this phase region, vesicles are easily aspirated and return to their quasi-spherical form after expiration. The elastic properties such as the bending rigidity [20,21] and area expansion modulus (Rowat, A.C., unpublished data) of fluid membranes containing 10 and 20 mol% farnesol can also be determined. At 13 °C, these farnesol–DMPC GUVs exhibit behaviour characteristic of a phase with solid properties. Deformations persist upon expiration and buckling folds are

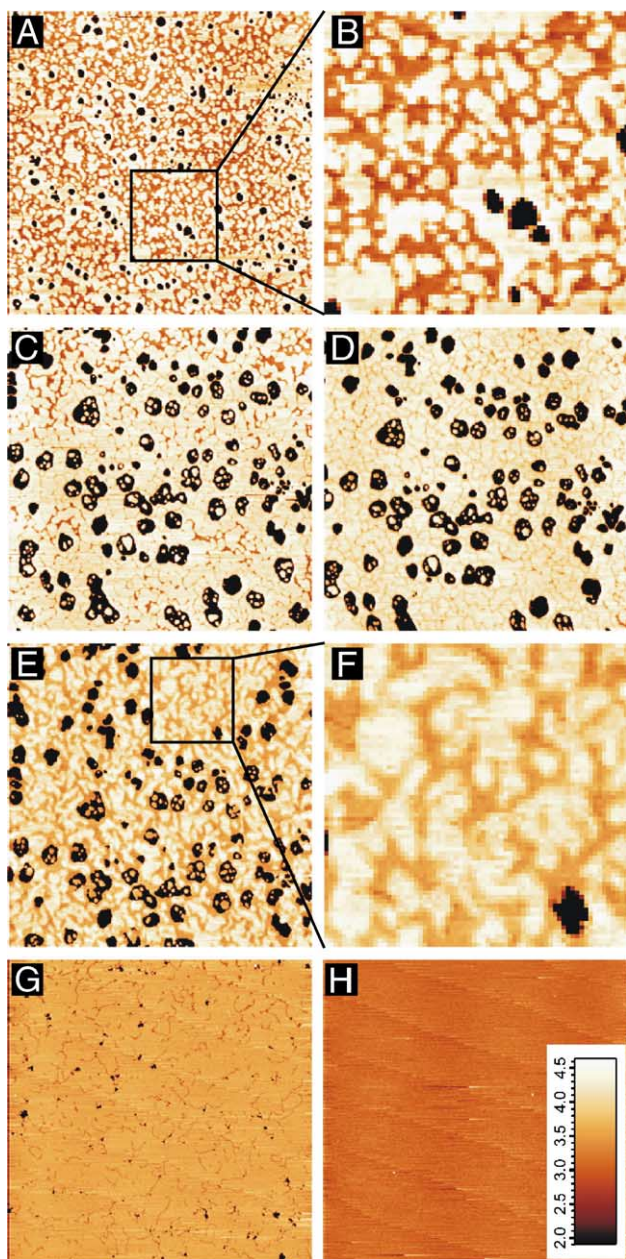


Fig. 4. AFM images of mica-supported DMPC+20 mol% farnesol bilayers at various temperatures in the heating experiment: A: 8.8 °C; B: magnification of A; C: 12.9 °C; D: 18.2 °C; E: 21.7 °C; F: magnification of E; G: 23.3 °C; and H: 35 °C. Images B and E are  $1.3 \times 1.3 \mu\text{m}^2$ . All other images are  $5 \times 5 \mu\text{m}^2$ .

observed upon vesicle failure (Fig. 5). Membrane mechanical properties are thus largely unaffected by the presence of up to 20 mol% farnesol.

#### 4. Discussion

In this study, we have sought to obtain a more complete understanding of how farnesol affects membrane physical properties. To achieve this, we have investigated farnesol–DMPC phase behaviour using DSC and AFM. We also

present evidence obtained by micropipette aspiration that membrane mechanical properties remain relatively unchanged despite the presence of farnesol.

##### 4.1. Phase diagram

DSC is useful in characterizing the thermodynamic behaviour of membranes and has been used to map out the phase boundaries for various lipid–lipid mixtures [32–35]. This technique, however, provides no direct structural information. Complementary evidence is obtained by AFM and micromechanics so that a more complete phase diagram can be constructed.

Descriptions of how we determined the temperature of the phase boundaries from the DSC thermograms of DMPC–farnesol dispersions and from the AFM images are documented in Materials and Methods. Correlating the temperatures of the phase boundaries from these two sources is challenging as the DSC experiments were performed on multilamellar vesicles and supported bilayers were imaged with AFM. It is well established that the interaction of bilayer and substrate increases the phase transition temperature of the upper leaflet and gives rise to a second transition corresponding to the transition of the lower leaflet that directly contacts the mica surface [28]. Indeed, AFM observations show that the temperature range of the main phase coexistence region for supported bilayers differs from that of vesicles.

For example, the main phase transition for DMPC+10 mol% farnesol extends from about 19 °C to 24 °C while the corresponding temperature range for vesicles observed by DSC is approximately 2 °C lower. Accounting for the differences in the temperature of the transition between supported bilayers and vesicles, the AFM images of lateral membrane organization provide structural evidence for the resulting phase diagram displayed in Fig. 6B.

With increasing concentrations of farnesol, there is a broadening of the pure lipid gel-to-fluid phase transition

Table 1  
Enthalpy of the main phase transition ( $\Delta H$ ) vs. farnesol concentration

Farnesol Concentration (mol%)	$\Delta H(\text{kJ/mol DMPC+farnesol})$	$\Delta H(\text{kJ/mol DMPC})$
0.0 (DMPC)	$14.4 \pm 0.3$	$14.4 \pm 0.3$
$2.9 \pm 0.2$	$17.5 \pm 0.4$	$17.9 \pm 0.4$
$5.6 \pm 0.2$	$19.8 \pm 0.6$	$20.9 \pm 0.6$
$8.2 \pm 0.3$	$15.6 \pm 0.2$	$16.9 \pm 0.2$
$10.8 \pm 0.3$	$15.1 \pm 0.9$	$16.8 \pm 0.9$
$13.0 \pm 0.7$	$13.6 \pm 0.3$	$15.5 \pm 0.3$
$15.2 \pm 0.7$	$14.8 \pm 2.1$	$17.5 \pm 2.1$
$19.3 \pm 0.7$		$9.1^* \pm 0.2$

Both the pre- and post-transitions are neglected in this determination of  $\Delta H$ .

\* At 19.3 mol% farnesol, the calorimetric scanning range may not capture all aspects of the main phase transition so the reported value for enthalpy (denoted by a star) may thus be lower than the actual enthalpy of transition. Above 19 mol% farnesol, the baseline could not be determined with great enough consistency to calculate  $\Delta H$ . Errors represent variations in  $\Delta H$  that result from integration over three different temperature bounds.

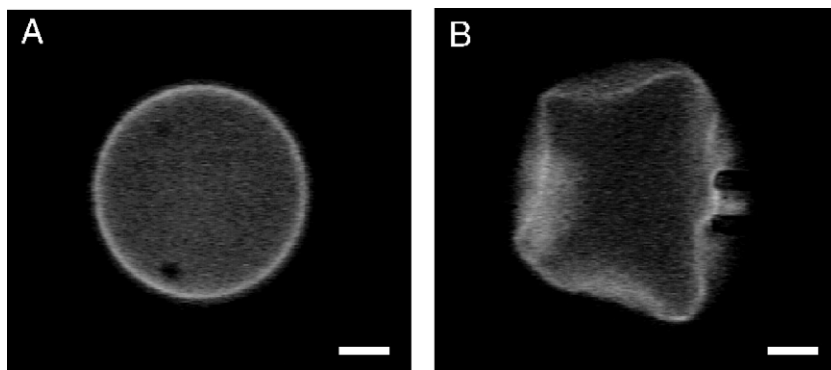


Fig. 5. (A) A DMPC vesicle containing 20 mol% farnesol and 0.1 mol% Di-I-C<sub>18</sub> at 13 °C. (B) Upon vesicle collapse, crumpling and buckling of the vesicle is observed. This mechanism of failure reveals characteristics of a solid, gel-phase membrane. Scale bar represents 5 μm.

into a gel–fluid ( $\mathcal{G}+f$ ) two-phase coexistence region (Fig. 6). This is shown via both DSC and AFM images of DMPC–farnesol supported bilayers. In this region of the phase diagram, DMPC–farnesol membranes containing 10 and 20 mol% farnesol exhibit two coexisting phases with a height difference of 7–8 Å. This is characteristic of the difference in height between a supported gel and fluid phase monolayer (Fig. 6B (i)) [27]. The domains are larger in size with 10 mol% farnesol compared to 20 mol%, but scale to similar branching shapes (Figs. 3C, 4F). The emergence of such a coexistence region is characteristic of a classical freezing point depression. While small concentrations of farnesol (2.9 mol%) reduce the temperature of the gel–fluid transition and induce a narrow coexistence region, there is also a slight increase in the enthalpy of the main transition. The origin of this increase is unclear but is indicative that the organization of farnesol in the  $f$  and  $\mathcal{G}$  phases differs and

that farnesol itself contributes to the entropy of the main transition. A previous study revealed a progressive decrease in the enthalpy of the main transition but no initial increase [18]. As discussed above, determining  $\Delta H$  is highly dependent upon the choice of baseline and thus may give rise to discrepancies in  $\Delta H$  values. Also at 2.9 mol% farnesol, a small shoulder begins to emerge on the upper temperature side of the  $C_p$  peak, whose form grows more pronounced with increasing farnesol concentration.

In the extended temperature range above the main peak, we observe that the small shoulder on the  $C_p$  curves becomes more defined at and above farnesol concentrations of 10.8 mol%. The origin of the heat represented in this shoulder is uncertain. On the phase diagram, we illustrate this feature by the region (Fig. 6B). We sought to clarify the nature of the  $\gamma$ -region using AFM. In the temperature range above, the gel–fluid coexistence region, we observed

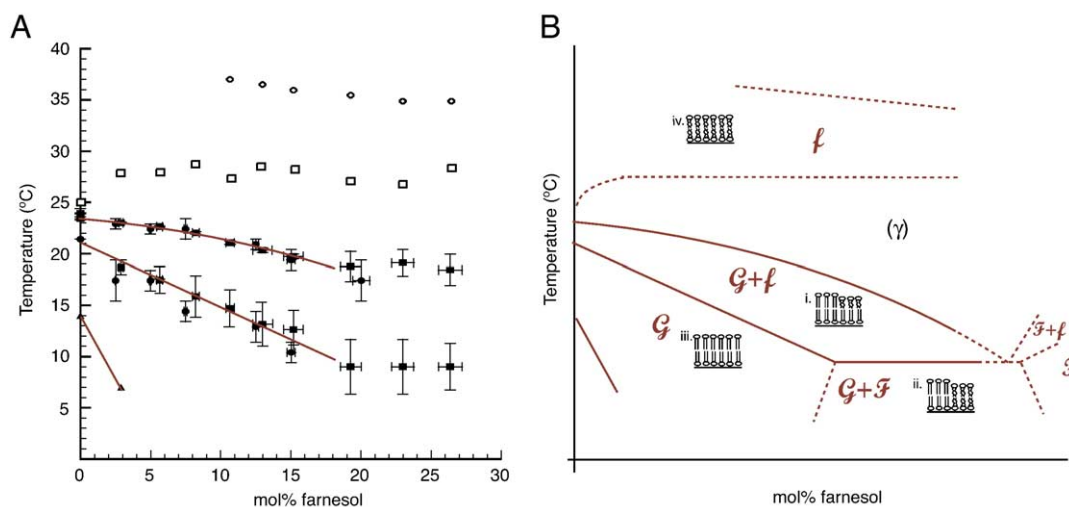


Fig. 6. Phase diagram of DMPC–farnesol compiled from the  $C_p$  curves and AFM images. (A) Data obtained by both DSC (DMPC–farnesol, solid squares) and <sup>2</sup>H NMR (DMPC-d<sub>54</sub>, solid circles reproduced with permission from Rowat and Davis, 2004) are in good agreement. Temperatures for DMPC-d<sub>54</sub>–farnesol have been corrected to  $T_m=24$  °C to account for the difference in  $T_m$  between DMPC and DMPC-d<sub>54</sub>. Error bars represent estimated error in the determination of the phase boundaries. (B) Proposed phase diagram. Phase boundaries correspond to the experimentally obtained data. Symbols represent:  $f$ , the fluid phase;  $\mathcal{F}$ , the farnesol-rich phase; and  $\mathcal{G}$ , the gel phase. Accompanying the phase diagram are schematic illustrations of the leaflet behaviour in supported bilayers visualized by AFM: (i)  $\mathcal{G}+f$ , typical gel–fluid coexistence in a supported bilayer; (ii)  $\mathcal{G}+f$ , coexistence of a gel (farnesol-poor) phase and fluid, farnesol-rich phase; (iii)  $\mathcal{G}$ , the gel phase where both lipid leaflets exhibit extended acyl chains; and (iv) above the gel–fluid coexistence region where both leaflets are in the fluid phase. Uncertainties in the nature and/or boundary of transitions are represented by stippled lines.

homogeneous lateral membrane organization characteristic of the fluid phase. With a lateral resolution of 10–20 nm and extreme sensitivity to differences in height ( $\sim\text{\AA}$ ) of a soft membrane, AFM provides evidence of only one average environment in this phase region. Nor did a previous  $^2\text{H}$  NMR study detect the coexistence of fluid phases larger than 100 nm [19]. Due to the uncertainty in the nature of the  $\gamma$ -region, it is represented by a stippled line in the phase diagram.

Above  $X_{\text{fsl}}=19$  mol%, the distinct peak has disappeared and a very broad transition is observed whose shape does not change significantly with increasing farnesol concentration. The invariance of this phase change at higher farnesol concentrations ( $X_{\text{fsl}}\geq 19$  mol%) supports the three-phase line in the phase diagram (Fig. 6B). Endotherms obtained by DSC are extremely broad and the enthalpy of this transition is less than that of the pure lipid gel-to-fluid transition. This indicates that the chain entropy of the two phases above and below the three-phase line is more similar than pure gel and fluid phases.

Our AFM studies shed light on the nature of the phase below the three-phase line. With 20 mol% farnesol, membranes in this phase region exhibit two coexisting phases with a height difference of 13–14  $\text{\AA}$ . This height difference is markedly different from that of the main gel–fluid ( $\mathcal{G}+f$ ) coexistence region (7–8  $\text{\AA}$ ) and shows that this phase region is distinct from the main coexistence region. Also, the domains in this region below the three-phase line are rounder in shape than those observed in the  $\mathcal{G}+f$  region with 10 and 20 mol% farnesol (Figs. 4B versus F). As depicted in Fig. 6B (ii), a height difference of 13–14  $\text{\AA}$  corresponds to lateral phase separation in both monolayers and indicates the presence of farnesol-rich fluid ( $\mathcal{F}$ ) and farnesol-poor ( $\mathcal{G}$ ) domains. This model is further substantiated by an analysis of the area of the two phases in the  $\mathcal{G}+\mathcal{F}$  coexistence region revealing that the farnesol-rich  $\mathcal{F}$  phase occupies about 40% of the surface area and the farnesol-poor ( $\mathcal{G}$ ) phase about 60% at  $T=8.8$  °C. As farnesol has a smaller cross-sectional area than a phospholipid and is present at a concentration of only 20 mol%, the fluid areas occupying 40% area must thus be composed of both lipids and farnesol. These observations provide further structural evidence of farnesol's preference for the fluid phase. Farnesol's tendency to promote the fluid phase is also demonstrated in the way the two-phase line demarcating the fluid phase and the two-phase coexistence region (fluidus boundary) extends to lower temperatures as the farnesol concentration is increased. Together, these observations of farnesol's preference for the fluid phase complement the existing knowledge of DMPC–farnesol phase behaviour [18,19].

Upon increasing the temperature, the farnesol-poor ( $\mathcal{G}$ ) phase increases in area at the expense of the farnesol-rich ( $\mathcal{F}$ ) phase. The observed area change happens gradually throughout the temperature range 6.4 to 18.2 °C and at a temperature of about 18.2 °C yields ordinary gel–fluid

coexistence with a 7–8  $\text{\AA}$  height difference (Fig. 6b (i)). At higher  $X_{\text{fsl}}$ , the  $\mathcal{G}+\mathcal{F}$  coexistence region must be bounded by the farnesol-rich phase,  $\mathcal{F}$ , according to Gibbs' phase rule. The precise boundaries at higher concentrations above 26 mol% farnesol are uncertain and are represented by stippled lines. Likewise, the exact boundary between  $\mathcal{G}+\mathcal{F}$  and the gel phase,  $\mathcal{G}$ , is unclear. We can estimate the form of this phase boundary by analyzing the change in the proportion of the area of the two phases in the DMPC+20 mol% farnesol membrane as a function of temperature. The Lever rule dictates that the proportion of the two phases along a tie line at constant temperature is a function of the distance from the endpoints (phase boundaries). In this way, we can predict the general topology of the phase boundaries of the  $\mathcal{G}+\mathcal{F}$  coexistence region. This region is bounded at lower concentrations by the  $\mathcal{G}$  phase. The notation  $\mathcal{G}$  is used to denote this phase region below the main  $\mathcal{G}+\mathcal{F}$  coexistence region where a gel phase with varying degrees of disorder is observed. Both the height of supported bilayers and mechanical properties of GUVs in this phase region are characteristic of a solid-like phase. At 13 °C, micropipette aspiration investigations of GUVs containing 10 mol% and 20 mol% farnesol reveal gel phase behaviour. At this temperature and with 10 mol% farnesol, membranes are in the  $\mathcal{G}$  phase region. At the same temperature and a concentration of 20 mol% farnesol, we are in the main  $\mathcal{G}+\mathcal{F}$  coexistence region near the solidus boundary where the membrane contains a large proportion of  $\mathcal{G}$  phase (Lever Rule). It is therefore not surprising that gel phase characteristics dominate membrane behaviour.

While exhibiting characteristics of a gel phase, varying degrees of reduced order and/or altered dynamics have been observed in the  $\mathcal{G}$  phase by spectroscopy [18,19]. An earlier  $^2\text{H}$  NMR study provided values of the first moments ( $M_1$ ), a sensitive measure of membrane phase, of farnesol–DMPC– $d_{54}$  mixtures.  $M_1$  values are proportional to spectral width so a decrease in  $M_1$  values is synonymous with a decrease in membrane order and/or alteration in the types of acyl chain motion. For temperatures and concentrations below the main two-phase region, the value of  $M_1$  decreases markedly with increasing farnesol concentration [19]. A similar decrease in DPH fluorescence anisotropy order parameters in extracted human leukemia *CeM-CI* cell membranes with farnesol has also been observed [18]. Both of these results reflect either an increase in the degree of molecular disorder within the gel phase, and/or significant changes in the rates and/or types of molecular motion which occur in the gel phase.

At concentrations of farnesol above 15.2 mol%, there is evidence of an additional transition with smaller enthalpy which lies above the main transition at about 35 °C. The nature of the phase above this transition is not clear. At higher temperatures (37 °C) beyond the  $\gamma$ -region, a slight decrease in the membrane bending rigidity,  $\kappa$ , was determined by vesicle fluctuation analysis (VFA) [20,21]. This observed minor reduction in  $\kappa$  may be attributed to density fluctuations between two coexisting subphases

[36,37] or may reflect farnesol's tendency to promote the fluid phase. This would correspond to a thinning of the membrane's hydrophobic core, decrease in acyl chain order, and area dilation. However, the quadrupolar splittings obtained by  $^2\text{H}$  NMR [19], which are proportional to the degree of acyl chain order [38] and correlated to the bilayer thickness [39,40], were found to be independent of farnesol concentration in the fluid phase and provide strong evidence that farnesol does not induce changes in acyl chain order above the main coexistence region. Elucidating the organization of farnesol in membranes requires further studies (molecular dynamics simulations, scattering).

#### 4.2. Liquid ordered and solid disordered?

The effects of farnesol on membranes have interesting parallels to another well-studied membrane component that also derives from the mevalonate synthesis pathway, cholesterol. Both cholesterol and farnesol have a similar interfacially anchoring hydroxyl group and size, but farnesol's isoprenoid chain is flexible with protruding methyl groups, whereas cholesterol's hydrophobic structure is rigid and smooth. The effects of cholesterol on membranes have been the subject of both experimental [41] and theoretical [42] investigations. This sterol is renowned for promoting the formation of a new liquid-ordered ( $L_o$ ) phase at high cholesterol content ( $X_{\text{chol}} \geq 20$  mol%) that has features of both the fluid phase (liquid disordered with lateral mobility, chain flexibility, and a zero shear modulus) and the gel phase (solid ordered with increased  $M_1$  values and acyl chain order) [42]. Despite increased  $M_1$  values and acyl chain order above  $T_m$  of the pure lipid, membranes containing cholesterol maintain mechanical properties characteristic of the fluid phase (zero shear modulus).

Farnesol, on the other hand, stabilizes the fluid phase without largely affecting the mechanical properties, lateral organization, and acyl chain order. Despite decreased  $M_1$  values and DPH anisotropy below  $T_m$  of the pure lipid, membranes containing farnesol maintain mechanical properties characteristic of the gel phase (non-zero shear modulus). It is obvious that the structural differences between farnesol and cholesterol have major implications for lipid packing and membrane properties.

#### 4.3. What we can learn from model membranes?

Farnesyl is one member of the prenyl family that posttranslationally attaches to proteins and is important for protein–membrane association. Here, we show that farnesol partitions into membranes without altering membrane stability. This indicates that a farnesyl chain can promote farnesylated protein–membrane associations (e.g., nuclear membrane-farnesylated lamin protein interactions) without perturbing lipid membrane properties. Other posttranslational protein modifiers include saturated fatty acid chains (palmitoyl, myristoyl) as well as cholesterol. Saturated

chains, such as myristic acid, have been observed to have an opposite effect to that of branched chains (farnesyl, geranylgeranyl) which decrease and broaden the main transition (Rowat, A.C., unpublished data). For example, myristic acid—roughly equivalent in length to farnesol but lacking the branched methyl group—is seen to *increase* and broaden the main transition with fatty acid concentration in that this molecule promotes lipid ordering and stabilizes the gel phase [35].

In this study, we observe domain formation in the gel–fluid coexistence region as well as at temperatures below this region in the phase diagram. Together with the topology of the phase diagram, this evidence shows that farnesol preferentially partitions into more fluid domains. In this way, lateral membrane heterogeneity can be driven by both the condensation of 'ordered' elements as well as the affinity of less ordered lipids such as farnesol for more fluid domains. Indeed, proteins/peptides attached to prenyl chains have been demonstrated to be excluded from more ordered lipid microdomains in both model systems [10,11,22] and in living cells [13]. Such lateral membrane heterogeneity plays a role in regulating the sorting and targeting of certain plasma membrane proteins and lipids [43,44]. Experiments and modelling to determine the relative affinities of farnesol for domains of varying degrees of order will provide further insights into the mechanisms of domain formation in biological membranes.

## 5. Conclusions

This investigation has elucidated how farnesol affects the phase behaviour and physical properties of DMPC bilayers from the perspectives of thermodynamics, lateral organization, and mechanical properties. We show that farnesol preferentially partitions into the fluid phase without altering membrane stability. Our results provide a more thorough understanding of farnesol–DMPC phase behaviour and facilitate the construction of a more complete phase diagram. These findings offer insights into how farnesol mediates prenylated protein–membrane association: with an affinity for the fluid phase, isoprenoids like farnesol function to regulate membrane lateral organization by preferentially partitioning prenylated proteins into less ordered lipid domains. Understanding the fundamentals of how farnesol affects membranes is important for advancing our knowledge of how membrane heterogeneity and farnesol can regulate biological function.

## Acknowledgements

Thanks to L.A. Duelund for calorimetric assistance and J.H. Davis for constructive discussions. This work was supported by a Julie Payette Scholarship from the Natural Sciences and Engineering Research Council of Canada

(ACR) and the Hasselblad Foundation. MEMPHYS-Centre for Biomembrane Physics is supported by the Danish National Research Foundation.

## References

- [1] F.P. Schiestl, M. Ayasse, H.F. Paulus, C. Löfstedt, B.S. Hansson, F. Ibarra, W. Francke, Sex pheromone mimicry in the early spider orchid (*Ophrys sphegodes*): patterns of hydrocarbons as the key mechanism for pollination by sexual deception, *J. Comp. Physiol.*, A 186 (2000) 567–574.
- [2] M.L. Anthony, M. Zhao, K.M. Brindle, Inhibition of phosphatidylcholine biosynthesis following induction of apoptosis in HL-60 cells, *J. Biol. Chem.* 274 (1999) 19686–19692.
- [3] M.M. Wright, A.L. Henneberry, T.A. Lagace, N.D. Ridgway, C.R. McMaster, Un-coupling farnesol-induced apoptosis from its inhibition of phosphatidylcholine synthesis, *J. Biol. Chem.* 276 (2001) 25254–25261.
- [4] Y.D. Burke, M.J. Stark, S.L. Roach, S.E. Sen, P.L. Crowell, Inhibition of pancreatic cancer growth by the dietary isoprenoids farnesol and geraniol, *Lipids* 32 (1997) 151–156.
- [5] B.F. Brehm-Stecher, E.A. Johnson, Sensitization of *Staphylococcus aureus* and *Escherichia coli* to antibiotics by the sesquiterpenoids nerolidol, farnesol, bisabolol, and apritone, *Antimicrob. Agents Chemother.* 47 (2003) 3357–3360.
- [6] H. Koo, M.F. Hayacibara, B.D. Schobel, J.A. Cury, P.L. Rosalen, Y.K. Park, A.M. Vacca-Smith, W.H. Bowen, Inhibition of *Streptococcus mutans* biofilm accumulation and polysaccharide production by apigenin and *tt*-farnesol, *J. Antimicrob. Chemother.* 52 (2003) 782–789.
- [7] J.B. Rouillet, U.C. Luft, H. Xue, J. Chapman, R. Bychkov, C.M. Rouillet, F.C. Luft, H. Haller, D.A. McCarron, Farnesol inhibits L-type Ca<sup>2+</sup> channels in vascular smooth muscle cells, *J. Biol. Chem.* 272 (1997) 32240–32246.
- [8] A. Bringmann, S.N. Skatchkov, F. Faude, V. Enzmann, A. Reichenbach, Farnesol modulates membrane currents in human retinal glial cells, *J. Neurosci. Res.* 62 (2000) 396–402.
- [9] M. Sinensky, Functional aspects of polyisoprenoid protein substituents: roles in protein–protein interaction and trafficking, *Biochim. Biophys. Acta* 1529 (2000) 203–209.
- [10] K.A. Melkonian, A.G. Ostermeyer, J.Z. Chen, M.G. Roth, D.A. Brown, Role of lipid modifications in targeting proteins to detergent-resistant membrane rafts. Many raft proteins are acylated, while few are prenylated, *J. Biol. Chem.* 274 (1999) 3910–3917.
- [11] S. Moffett, D.A. Brown, M.E. Linder, Lipid-dependent targeting of G proteins into rafts, *J. Biol. Chem.* 275 (2000) 2191–2198.
- [12] J.R. Silvius, Lipidated peptides as tools for understanding the membrane interactions of lipid-modified proteins, *Curr. Top. Membr.* 52 (2002) 371–395.
- [13] D.A. Zacharias, J.D. Violin, A.C. Newton, R.Y. Tsien, Partitioning of lipid-modified monomeric GFPs into membrane microdomains of live cells, *Science* 296 (2002) 913–916.
- [14] M.A. McCloskey, F.A. Troy, Paramagnetic isoprenoid carrier lipids: 1. Chemical synthesis and incorporation into model membranes, *Biochemistry* 19 (1980) 2056–2060.
- [15] M.A. McCloskey, F.A. Troy, Paramagnetic isoprenoid carrier lipids: 2. Dispersion and dynamics in lipid membranes, *Biochemistry* 19 (1980) 2061–2066.
- [16] J.S. de Ropp, F.A. Troy, Chemical synthesis and <sup>2</sup>H NMR investigations of polyisoprenols: dynamics in model membranes, *Biochemistry* 23 (1984) 2691–2695.
- [17] J.S. de Ropp, F.A. Troy, <sup>2</sup>H-NMR investigation of the organization and dynamics of polyisoprenols in membranes, *J. Biol. Chem.* 260 (1985) 15669–15674.
- [18] O.P. Bondar, G. Melnykovyck, E.S. Rowe, Effects of farnesol on the thermotropic behaviour of dimyristoylphosphatidylcholine, *Chem. Phys. Lipids* 74 (1994) 93–98.
- [19] A.C. Rowat, J.H. Davis, Farnesol–DMPC phase behaviour: a <sup>2</sup>H NMR study, *Biochim. Biophys. Acta* 1661 (2004) 178–187.
- [20] A.C. Rowat, P.L. Hansen, J.H. Ipsen, Experimental evidence of the electrostatic contribution to membrane bending rigidity, *Europhys. Lett.* 67 (2004) 144–149.
- [21] A.C. Rowat, J. Brask, T. Sparrmann, K.J. Jensen, G. Lindblom, J.H. Ipsen, Farnesylated peptides in model membranes: a biophysical investigation, *Eur. Biophys. J.* 33 (2004) 300–309.
- [22] K. Lohner, A. Latal, G. Degovics, P. Garidel, Packing characteristics of a model system mimicking cytoplasmic bacterial membranes, *Chem. Phys. Lipids* 111 (2001) 177–192.
- [23] M.I. Angelova, D.S. Dimitrov, Liposome electroformation, *Faraday Discuss. Chem. Soc.* 81 (1986) 303–311.
- [24] M.I. Angelova, S. Soléau, P. Méléard, J.F. Faucon, P. Bothorel, Preparation of giant vesicles by external AC electric fields. Kinetics and applications, *Prog. Colloid & Polym. Sci.* 89 (1992) 127–131.
- [25] P.Y. Wang, J.W. Chen, F. Hwang, Anisodamine causes acyl chain interdigitation in phosphatidylglycerol, *FEBS Lett.* 332 (1993) 193–196.
- [26] T.B. Pedersen, S. Frokjaer, O.G. Mouritsen, K. Jorgensen, A calorimetric study of phosphocholine membranes mixed with desmopressin and its diacylated prodrug derivative (DPP), *Int. J. Pharm.* 233 (2002) 199–206.
- [27] D. Keller, N.B. Larsen, I.M. Møller, O.G. Mouritsen, Decoupled phase transitions and grain-boundary melting in supported phospholipid bilayers, *Phys. Rev. Lett.* 94 (2005) 025701.
- [28] J. Yang, J. Appleyard, The main phase transition of mica-supported phosphatidyl–choline membranes, *J. Phys. Chem., B* 104 (2000) 8097–8100.
- [29] W.L.C. Vaz, E.C.C. Melo, T.E. Thompson, Translational diffusion and fluid domain connectivity in a two-component, two-phase phospholipid bilayer, *Biophys. J.* 56 (1989) 869–876.
- [30] M.C. Giocondi, L. Pacheco, P.E. Milhiet, C.L. Grimellec, Temperature dependence of the topology of supported dimyristoyl–distearoyl phosphatidylcholine bilayers, *Ultramicroscopy* 86 (2001) 151–157.
- [31] L.K. Nielsen, T. Bjørnholm, O.G. Mouritsen, Critical phenomena: fluctuations caught in the act, *Nature* 404 (2000) 352.
- [32] S. Mabrey, J.M. Sturtevant, Investigation of phase transitions of lipids and lipid mixtures by high sensitivity differential scanning calorimetry, *Proc. Natl. Acad. Sci.* 73 (1976) 3862–3866.
- [33] K.M.W. Keough, P.J. Davis, Gel to liquid–crystalline phase transitions in water dispersions of saturated mixed-acid phosphatidylcholines, *Biochemistry* 18 (1979) 1453–1459.
- [34] J.R. Silvius, J. Gagné, Lipid phase behaviour and calcium-induced fusion of phosphatidylethanolamine–phosphatidylserine vesicles. Calorimetric and fusion studies, *Biochemistry* 23 (1984) 3232–3240.
- [35] R. Koynova, B. Tenchov, G. Rapp, Mixing behaviour of saturated short-chain phosphatidylcholines and fatty acids: eutectic points, liquid and solid phase immiscibility, non-lamellar phases, *Chem. Phys. Lipids* 88 (1997) 45–61.
- [36] T. Hønger, K. Mortensen, J.H. Ipsen, J. Lemmich, R. Bauer, O.G. Mouritsen, Anomalous swelling of multilamellar lipid bilayers in the transition region by renormalization of curvature elasticity, *Phys. Rev. Lett.* 72 (1994) 3911–3914.
- [37] L. Fernandez-Puente, I. Bivas, M.D. Mitov, P. Méléard, Temperature and chain length effects on bending elasticity of phosphatidylcholine bilayers, *Europhys. Lett.* 28 (1994) 181–186.
- [38] J.H. Davis, The description of membrane lipid conformation, order, and dynamics by <sup>2</sup>H-NMR, *Biochim. Biophys. Acta* 737 (1983) 117–171.
- [39] J.H. Ipsen, O.G. Mouritsen, M. Bloom, Relationships between lipid membrane area, hydrophobic thickness, and acyl-chain

- orientational order: the effects of cholesterol, *Biophys. J.* 57 (1990) 405–412.
- [40] H. Schindler, J. Seelig, Deuterium order parameters in relation to thermodynamic properties of a phospholipid bilayer. A statistical mechanical interpretation, *Biochemistry* 14 (1975) 2283–2287.
- [41] P.F.F. Almeida, W.L.C. Vaz, T.E. Thompson, Lateral diffusion in the liquid phases of dimyristoylphosphatidylcholine/cholesterol lipid bilayers: a free volume analysis, *Biochemistry* 31 (1992) 6739–6747.
- [42] J.H. Ipsen, G. Karlström, O.G. Mouritsen, H. Wennerström, M.J. Zuckermann, Phase equilibria in the phosphatidylcholine–cholesterol system, *Biochim. Biophys. Acta* 905 (1987) 162–172.
- [43] D.A. Brown, E. London, Structure and function of sphingolipid- and cholesterol-rich membrane rafts, *J. Biol. Chem.* 275 (2000) 17221–17224.
- [44] E. Ikonen, Roles of lipid rafts in membrane transport, *Curr. Opin. Cell Biol.* 13 (2001) 470–477.